

## ORIGINAL ARTICLE

## MiR-29b replacement inhibits proteasomes and disrupts aggresome+autophagosome formation to enhance the antimyeloma benefit of bortezomib

S Jagannathan<sup>1,2</sup>, N Vad<sup>1,2</sup>, S Vallabhapurapu<sup>3</sup>, S Vallabhapurapu<sup>3</sup>, KC Anderson<sup>4</sup> and JJ Driscoll<sup>1,2,3</sup>

Evading apoptosis is a cancer hallmark that remains a serious obstacle in current treatment approaches. Although proteasome inhibitors (PIs) have transformed management of multiple myeloma (MM), drug resistance emerges through induction of the aggresome+autophagy pathway as a compensatory protein clearance mechanism. Genome-wide profiling identified microRNAs (miRs) differentially expressed in bortezomib-resistant myeloma cells compared with drug-naïve cells. The effect of individual miRs on proteasomal degradation of short-lived fluorescent reporter proteins was then determined in live cells. MiR-29b was significantly reduced in bortezomib-resistant cells as well as in cells resistant to second-generation PIs carfilzomib and ixazomib. Luciferase reporter assays demonstrated that miR-29b targeted *PSME4* that encodes the proteasome activator PA200. Synthetically engineered miR-29b replacements impaired the growth of myeloma cells, patient tumor cells and xenotransplants. MiR-29b replacements also decreased PA200 association with proteasomes, reduced the proteasome's peptidase activity and inhibited ornithine decarboxylase turnover, a proteasome substrate degraded through ubiquitin-independent mechanisms. Immunofluorescence studies revealed that miR-29b replacements enhanced the bortezomib-induced accumulation of ubiquitinated proteins but did not reveal aggresome or autophagosome formation. Taken together, our study identifies miR-29b replacements as the first-in-class miR-based PIs that also disrupt the autophagy pathway and highlight their potential to synergistically enhance the antimyeloma effect of bortezomib.

*Leukemia* (2015) 29, 727–738; doi:10.1038/leu.2014.279

## INTRODUCTION

MicroRNAs (miRs) are noncoding RNAs that control gene expression and are deregulated in many human cancers.<sup>1,2</sup> Alteration in miR expression is linked to tumorigenesis and expression profiling has identified miR signatures associated with cancer diagnosis, staging and therapeutic response.<sup>3</sup> Loss of a tumor-suppressive miR activates inherently oncogenic pathways to promote cancer phenotypes and drug resistance.<sup>4,5</sup> The rationale to develop miR therapeutics is based upon the premise that aberrantly expressed miRs have key roles in cancer and that correcting these deficiencies by restoring miR function may provide therapeutic benefit.<sup>6</sup>

The ubiquitin (Ub)+proteasome system (UPS) maintains proteostasis by degrading misfolded and short-lived proteins.<sup>7</sup> The proteasome is the catalytic core of the UPS, and pharmacologic inhibition of the proteasome induces cancer cell death.<sup>8</sup> Proteasome inhibitors (PIs) have been exploited for therapeutic gain to treat multiple myeloma (MM) and yield durable responses that enhance survival.<sup>9,10</sup> Bortezomib (Velcade, Millennium-Takeda Oncology, Cambridge, MA, USA) has emerged as the standard-of-care for MM but serious obstacles remain.<sup>11</sup> Many patients do not respond to PIs; those who do respond inevitably develop resistance and the molecular bases of patient susceptibility remains unknown.<sup>12–14</sup> Moreover, next-generation PIs possess

their own adverse effects and are unlikely to provide long-term benefit without the development of drug resistance.

Drug resistance still accounts for the majority of tumor relapses and cancer-related deaths. Whereas bortezomib promotes the accumulation of polyubiquitinated proteins, it also induces aggresome and autophagosome formation to promote protein clearance, tumor survival and relative drug resistance. Pharmacologic inhibition of both proteasomes and autophagy offers great potential to overcome therapeutic resistance. Here, we demonstrate that miR-29b represses *PSME4* to inhibit proteasomes but, in contrast to bortezomib, does not induce aggresome or autophagosome formation. Hence, miRs may offer a therapeutic advantage for myeloma treatment by inhibiting proteasomes without inducing pro-survival autophagy.

## MATERIALS AND METHODS

## Cells and reagents

MM cell lines were grown in complete RPMI and AMCL1, AMCL2 and Waldenström's macroglobulinemia cells (Massachusetts General Hospital, Boston, MA, USA) in complete DMEM. Bortezomib, carfilzomib and ixazomib were from Selleck Chemicals (Houston, TX, USA), succinyl-Leu-Leu-Val-Tyr-MCA (Suc-LLVY-MCA) and XTT (sodium 2,3-bis(2-methoxy-4-nitro-5-sulfophenyl)-5-[(phenylamino)carbonyl]-2H-tetrazolium) (Sigma, St Louis, MO, USA)

<sup>1</sup>The Vontz Center for Molecular Studies, University of Cincinnati College of Medicine, Cincinnati, OH, USA; <sup>2</sup>Division of Hematology and Oncology, The Vontz Center for Molecular Studies, University of Cincinnati College of Medicine, Cincinnati, OH, USA; <sup>3</sup>Department of Cancer Biology, University of Cincinnati College of Medicine, Cincinnati, OH, USA and <sup>4</sup>Jerome Lipper Multiple Myeloma Center and LeBow Institute for Myeloma Therapeutics, Dana-Farber Cancer Institute, Harvard Medical School, Boston, MA, USA. Correspondence: Professor JJ Driscoll, Division of Hematology and Oncology, The Vontz Center for Molecular Studies, University of Cincinnati College of Medicine, 3125 Eden Avenue, Cincinnati, OH 45267, USA.

E-mail: driscojs@uc.edu

Received 26 June 2014; revised 22 August 2014; accepted 2 September 2014; accepted article preview online 19 September 2014; advance online publication, 14 October 2014

and miR replacements/antagomirs (Switchgear Genomics, Menlo Park, CA, USA).

#### Live-cell measurement of proteasome activity

The short-lived fluorescent reporter GFPu was constructed by fusing a 16-amino-acid degradation signal to green-fluorescent protein (GFP)<sup>15</sup> (Clontech, Mountain View, CA, USA). Human embryonic kidney cells were stably transfected with GFPu.

#### MiR replacements/antagomir transfection

Replacements/antagomirs were transfected into target cells using Lipofectamine RNAimax (Invitrogen, Carlsbad, CA, USA). MiRs were diluted in Opti-MEM, mixed with RNAimax and added dropwise.

#### Transduction of miR-expressing lentivirus

Lentivirus vectors (SBI Biosystems, Mountain View, CA, USA) that expressed scrambled or experimental miRs were transfected with packaging vector, pPACKH, into 293T cells using Lipofectamine 2000 (Invitrogen). After 48 h, the virus was collected and RPMI8226 cells transduced with vectors expressing scrambled miR, miR-29b or miR-29b. Those lacking the nuclear localization signal (NLS) were designated miR-29bΔNLS. Cells were mixed with virus and polybrene (8 μg/ml), centrifuged at 2000 r.p.m. for 90 min, incubated overnight, media changed and selected in puromycin.

#### Viability assay

Cells (200 μl) were plated, transfected with miRs, incubated for 72 h and activated XTT was added. Absorbance was determined using a BMG Labtech OPTIMA plate reader (BMG Labtech Inc., Cary, NC, USA).

#### Quantitation of fluorescence

Cells were transfected with miRs and incubated for 48 h. Bortezomib was added, cells were incubated for 16 h and visualized using a Zeiss LSM 170 confocal microscope with Axio Observer Z1 (Zeiss Microscopy, Jena, Germany). Fluorescence was quantified using ImageJ (NIH, Bethesda, MD, USA) and normalized relative to vehicle-treated cells.

#### Nuclear factor-kappaB (NFκ-B) activity

Cells were transduced with plasmids expressing *G-Luc* under NFκ-B, cytomegalovirus or SV40 promoter control. Cells were then transfected with control or experimental miRs (20 nM), grown for 24 h, split into equal portions and one-half was treated with 10 ng/ml tumor necrosis factor-α (TNF-α). Cells were incubated for 16 h and luminescence determined from the media using BMG Labtech FLUOstar OPTIMA after the addition of Gar2 reagent and 1 × supplement.<sup>16,17</sup>

#### Proliferation assay

The miR effect on proliferation was determined using the 5-bromo-2'-deoxyuridine (BrdU) kit (Cell Signaling Technology, Danvers, MA, USA) to detect incorporation of BrdU into the newly synthesized DNA. RPMI8226 cells were labeled using BrdU-containing media, fixed, DNA denatured and mouse anti-BrdU monoclonal antibody was added. Anti-mouse IgG horseradish peroxidase (HRP)-linked antibody detected bound anti-BrdU ab. The HRP substrate TMB (3,3',5,5'-tetramethylbenzidine) was added as a color developer and absorbance was proportional to the incorporated BrdU and proliferation.

#### Methylcellulose colony formation assay

Cells transduced with miR-expressing lentiviral vectors were plated in 1.27% methylcellulose. After 9 days, colonies were counted using a Nikon (Nikon Inc., Melville, NY, USA) eclipse TE200 bright field microscope. Colonies with < 10 cells were excluded.

#### Apoptosis assay

Cells were transfected with miRs, incubated for indicated times at 37 °C and 5% CO<sub>2</sub>. Cells were then collected and centrifuged at 200 g for 5 min. The supernatant was discarded and the pellet was washed with 1 × buffer. Cells were then resuspended in 90 μl of 1 × buffer and 10 μl of fluorescein isothiocyanate-conjugated annexin V (Molecular Probes, Grand Island, NY,

USA), incubated in the dark and analyzed using a Coulter epics XL-MCL (Beckman-Coulter Inc., Brea, CA, USA).

#### Real-time (RT) measurements

Longitudinal analysis of cell confluency was determined using the Incucyte Zoom second-generation live-cell kinetic imaging system and software (Essen Bioscience, Ann Arbor, MI, USA) integrated with a cell culture incubator. RPMI8226 cells were transduced with miR, incubated for 48 h, bortezomib added and images acquired every 2 h over 48 h. Confluence and cells/mm<sup>2</sup> were quantified.

#### Western blot

In all, 1 × 10<sup>6</sup> cells were placed in six-well plates and transfected with scrambled control or experimental miRs. Cells were collected, centrifuged at 200 g for 8 min, the supernatant discarded and the pellet washed with 1 × phosphate-buffered saline (PBS). The pellet was resuspended in RIPA buffer, lysed and centrifuged at 12 000 g for 10 min. Protein concentration of the lysate was determined using the Pierce BCA Protein Assay Kit (Thermo-Scientific, Florence, KY, USA). Samples (20 μg) were electrophoresed on 5–20% gels (Wako Chemicals, Richmond, VA, USA) in the XCell mini-cell system (Invitrogen). Proteins were transferred to nitrocellulose and incubated with Odyssey (LI-COR, Lincoln, NE, USA) blocking buffer for 30 min followed by 1° antibodies (1:1000) for 16 h at 4 °C. Membranes were washed thrice in PBS-Tween-20 (PBS-T, 0.05%), incubated for 30 min with IR Dye 2° antibody (1:5000) and visualized using the Odyssey infrared imaging system.

#### Subcellular fractionation

293T cells were transfected with control or miR replacements, lysates were prepared and nuclear and cytoplasmic fractions were separated (Invitrogen).

#### Generation of PI-resistant cell lines

RPMI8226 cells were grown under standard conditions and exposed to successively increased concentrations of the PIs bortezomib, carfilzomib or ixazomib over 6 months to generate PI-resistant cells. As controls, parental cells were exposed to dimethylsulphoxide vehicle under the same algorithm as resistant cells.

#### Nondenaturing gel electrophoresis

RPMI8226 cells were transfected with scrambled miR, miR-29b or miR-29bΔNLS replacements and incubated +/- bortezomib. Gels were incubated in 25 mM Tris-HCl (pH 7.4) 3 mM ATP, 5 mM MgCl<sub>2</sub> and Suc-LLVY-MCA at 37 °C, and free AMC (7-amino-4-methylcoumarin) was visualized using a UV transilluminator.

## RESULTS

Whereas the therapeutic benefit of bortezomib remains unchallenged, acquired drug resistance remains a major obstacle toward achieving sustained clinical responses. As the molecular basis of PI resistance remains poorly defined, we exposed drug-sensitive myeloma cells to successively increased concentrations of bortezomib to generate drug-resistant cells that displayed IC<sub>50</sub> values more than fivefold greater than that determined for parental cells (Supplementary Figure 1). We then identified miRs differentially expressed in the bortezomib-resistant cells. Over > 15 000 pre-miR and mature miR were screened; however, only 26 human miRs were expressed with statistical difference between bortezomib-resistant and parental cells (Supplementary Table 1). MiR-17–92 displayed the greatest increase in expression in bortezomib-resistant cells, whereas miR-29 family members miR-92-1, miR-21 and miR27 were significantly reduced relative to parental cells and have been linked to tumorigenesis.<sup>18,19</sup> To investigate the biological effect of miRs differentially expressed in bortezomib-resistant cells, miR replacements were synthetically engineered to mimic those miRs increased in bortezomib-resistant cells and synthetic

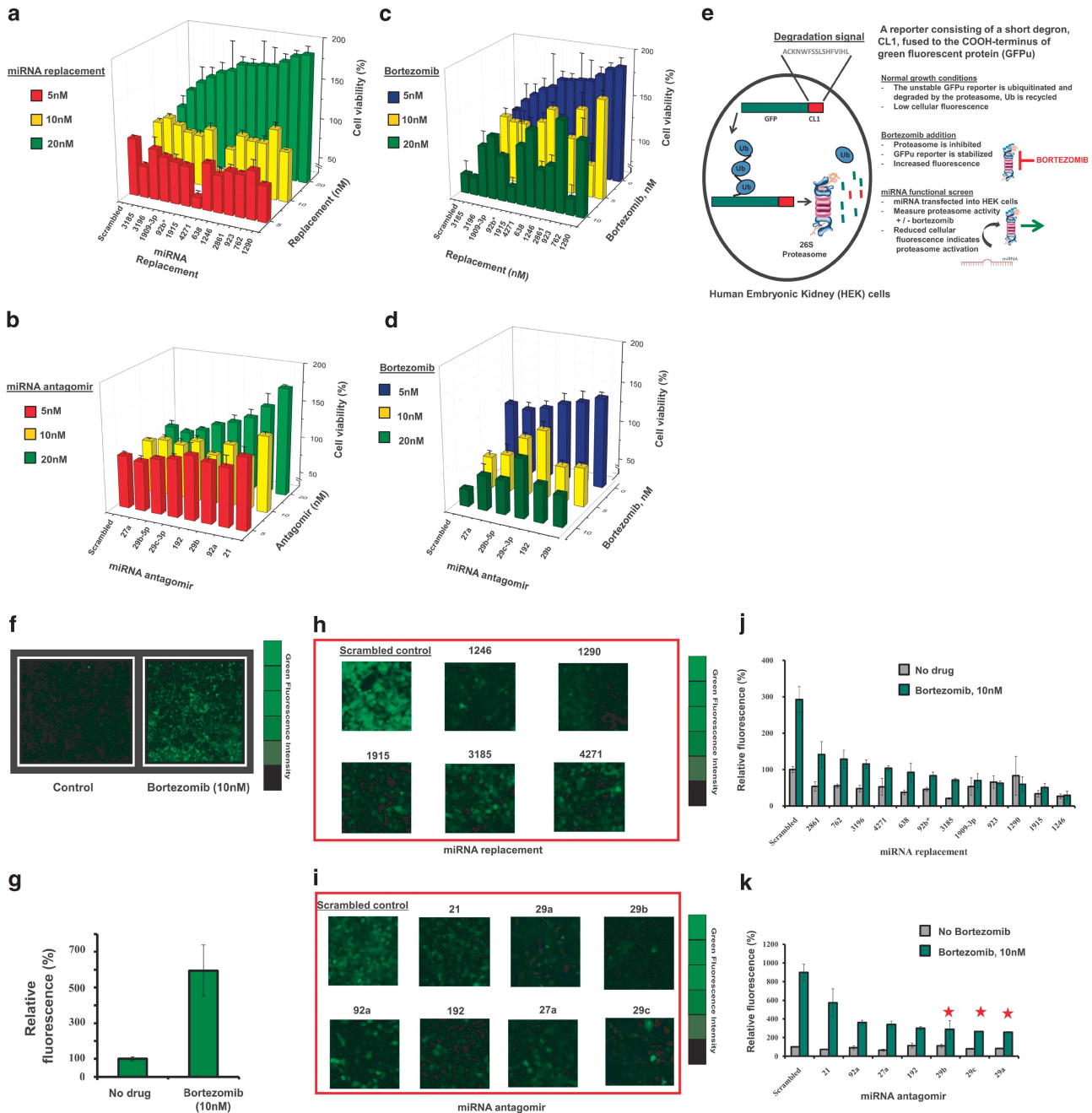


**Figure 1.** Identification of miRs that control UPS activity. **(a)** MiR replacement effect on viability. Cells were transfected with replacements at and viability determined using the XTT assay. Shown is the average of triplicate measurements. **(b)** Antagomir effect on viability. **(c)** MiR replacement effect on viability in the presence of bortezomib. Cells were transfected with replacements at indicated concentrations, cultured for 48 h and then treated with bortezomib at indicated concentrations. **(d)** Antagomir effect on viability in the presence of bortezomib. Cells were transfected with antagonists at indicated concentrations, cultured for 48 h and then treated with bortezomib at indicated concentrations. **(e)** Scheme for functional screening to quantitate the miR effect on proteasome activity in human embryonic kidney (HEK) cells stably transfected with GFPu. **(f)** Bortezomib effect on GFPu accumulation. HEK cells were treated with bortezomib for 16 h and imaged using confocal microscopy. **(g)** Quantitation of the bortezomib effect on HEK cells. Relative fluorescence was determined using the ImageJ image processing and analysis software. **(h)** Effect of bortezomib on fluorescence in HEK cells transfected with control or miR replacements. Cells were transfected with indicated miRs, cultured for 48 h and treated with bortezomib. **(i)** Effect of bortezomib on fluorescence in HEK cells transfected with scrambled control or miR antagonists. Cells were transfected with indicated miRs, cultured for 48 h and treated with bortezomib for 16 h. **(j)** Quantitation of miR replacement effect on cell fluorescence after bortezomib treatment. Relative fluorescence was determined using the ImageJ processing and analysis software. **(k)** Quantitation of antagomir effect on fluorescence after bortezomib treatment. Relative fluorescence was determined using the ImageJ image processing and analysis software. ★ denotes members of the miR-29b family.

antagonists were designed by base-pair complementarity to inhibit those miRs reduced in bortezomib-resistant cells. Replacements or antagonists were transfected into myeloma cells and the effect on viability was determined

(Figures 1a and b). Twelve miR replacements and five antagonists increased myeloma viability in a dose-dependent manner. MiR replacements 1290, 762, 923, 2861, 1246, 638 and 4271 and antagonists of miRs 29b, 29c, 192 and 27a also

promoted myeloma viability in the presence of bortezomib (Figures 1c and d).

Numerous mechanisms have been proposed to explain the molecular basis for bortezomib resistance; however, a limited number of these directly address the functional or structural properties of the proteasome. Whereas biochemical assays are useful in rapidly assessing the functional status of the proteasome, such assays do not incorporate the intricacy of substrate passage through the many physiologically relevant steps within the UPS. We reasoned that a live-cell system that employed a short-lived reporter offered a more satisfactory means to assess miR effects on the UPS. Proteasome activity was monitored by the fluorescence emitted from cells that expressed GFPu (Figure 1e). After MG132 treatment, GFPu is co-immunoprecipitated with Ub and pulse-chase experiments indicated that the GFPu half-life is significantly increased upon proteasome inhibition.<sup>20</sup> Human

embryonic kidney cells were transfected with GFPu, treated with bortezomib and fluorescence was measured with confocal imaging. After bortezomib treatment, we saw an approximately sixfold increase in fluorescence compared with cells treated with vehicle alone (Figures 1f and g). GFPu-expressing human embryonic kidney cells were then transfected with individual replacements or antagomirs, treated with bortezomib and fluorescence was measured (Figures 1h and i). In contrast to control-transfected cells, fluorescence from cells transfected with miR replacements 1246, 1290, 1915, 3185 and 4271 did not significantly increase after bortezomib treatment to suggest that the miRs promoted flux through the UPS and GFPu degradation even in the presence of bortezomib (Figure 1j). Fluorescence from cells transfected with antagomirs designed to reduce the endogenous levels of miR-21, 27a, 29a, 29b, 29c, 92a and 192 did not increase with bortezomib (Figure 1k).

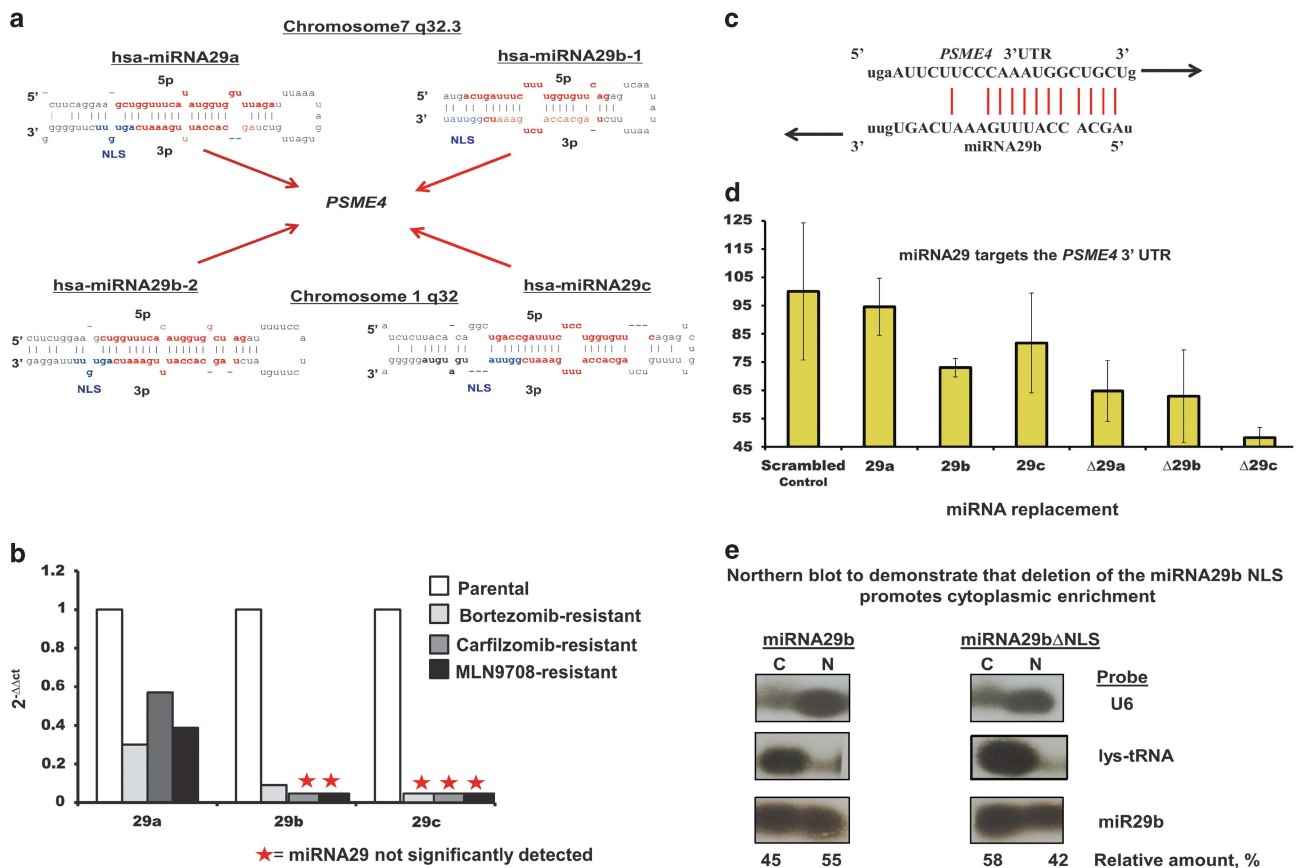


**Figure 2.** MiR-29b targets *PSME4*. (a) Nucleotide sequence of the mature pre-miRNAs that are processed to generate miR-29a and 29b1 from chromosome 7 and miR-29b2 and 29c from Chromosome 1. The putative hexanucleotide NLS in each member is shown in blue. (b) RT-PCR quantitation of miR-29 in parental and PI-resistant cells. (c) MiR-29b complementarity to *PSME4* that encodes the proteasome activator PA200. (d) Luciferase readout demonstrating that miR-29 family members specifically target the *PSME4* 3'-UTR. MiRNAs reduced in cells resistant to PIs were identified. On the basis of predictive algorithms, putative binding to sites within the 3'-UTR of *PSME4* were determined. MiR 3'-UTR target clones and luciferase-based readout. The *PSME4* 3'-UTR was inserted into pEZ-MT01, a dual firefly/renilla dual luciferase reporter mammalian expression vector (GeneCopoeia, Rockville, MD, USA). Either the *PSME4* 3'-UTR-specific or empty vector control (pEZ-MT01 alone) were then transfected in HEK-293T target cells. MiR 3'-UTR target clones were used for miR target identification and functional validation of the predicted targets or to study the regulatory effect of miR on target gene(s). The *PSME4* 3'-UTR sequence was inserted downstream of the firefly luciferase included on miTarget 3'-UTR target clones, driven by the SV40 enhancer. Downstream of the miR 3'-UTR target reporter is the renilla luciferase reporter driven by a cytomegalovirus (CMV) promoter, which is also cloned into pEZX-MT01 that serves as the internal control. HEK293 cells were plated on a six-well plate, transfected with 1 µg of *PSME4* 3'-UTR miR target sequence expression clone in pEZX-MT01 vector with Luc and 20 nM of chemically synthesized miRs. Cells were transferred to a 96-well plate 18 h after transfection and cultured for 24 h. Both firefly luciferase and Renilla luciferase activities were measured and data were recorded on BMG Labtech FLUOstar OPTIMA. Firefly luciferase activity was then normalized with the renilla luciferase activities in the same well. (e) Northern blot analysis to determine the effect of deletion of the miR-29b NLS on subcellular localization. 293T cells transfected with control or the experimental miR replacements were harvested, lysates were prepared and separated into nuclear and cytoplasmic fractions. The efficiency of transfection was verified by subjecting the plasmids to northern blot analysis and probing with either tRNA<sup>lys</sup> (cytoplasmic fraction) or U6 small nuclear RNA (snRNA) (nuclear fraction). Oligonucleotide probes were 5' end-labeled with digoxigenin (DIG). ★ denotes that miR-29b was not significantly detected.



Genomic and functional screening indicated that miR-29a and 29b-1 (chromosome 7q32.3) and miR-29b2 and 29c (chromosome 1q32) were reduced in bortezomib-resistant cells (Figure 2a). MiR-29a/b/c share extensive homology within the 3'-untranscribed region (UTR) seed sequence that binds target mRNAs. Clinical success of bortezomib has led to the development of second-generation PIs, and RPMI8226 cells resistant to carfilzomib or ixazomib were then generated through successive drug exposure. RT-polymerase chain reaction (RT-PCR) indicated that miR-29a, 29b and 29c were each reduced in bortezomib-, carfilzomib- and ixazomib-resistant cells compared with the parental cells (Figure 2b). Predictive algorithms and database analyses identified mRNAs potentially targeted by miR-29b. On the basis of sequence complementarity and calculated miRSVR scores, 6995 putative mRNA targets of miR-29b were detected. We focused on UPS components as putative miR-29 targets, as it appeared reasonable to be used as a direct mechanism to promote PI resistance. Comparison of miRSVR scores for miR-29b targets revealed that *PSME4*, which encodes the proteasome activator PA200, was  $-1.35$  and ranked *PSME4* in the top 1% (73rd out of 6995) as a miR-29 target. Similarly,  $\sim 1100$  human miRs were rank ordered based upon their summed miRSVR scores as putative miRs that targeted *PSME4*. On the basis of predictive miRSVR scores, miR-29b and 29c ranked 5th and 6th highest, respectively, as miRs most likely to target *PSME4*. Moreover, the miRSVR score for *PSME4* was more significant than that of *DNMT3a* ( $-1.22$ ) and *DNMT3b* ( $-1.21$ ), previously been reported as miR-29b targets.<sup>21</sup> The *PSME4* 3'-UTR is homologous to the miR-29b seed sequence (Figure 2c) and the miR-29b replacement effect on *PSME4* expression was determined. A vector that encoded the *PSME4* 3'-UTR controlled by the renilla luciferase reporter and firefly luciferase normalization genes was transfected into 293T cells. MiR-29b and 29c replacements significantly reduced luciferase-generated fluorescent readout from the reporter by  $>40\%$  relative to the control vector. *PSME4* expression was highly sensitive to miR-29b (Figure 2d) and supported the findings that miR-29b modulated proteasome activity (Figures 1c and d). MiRs function through negative regulation of gene expression, in part, through partial sequence complementarity to target mRNAs. However, miRs may also contain additional sequence elements that control their functional activity, post-transcriptional behavior and/or subcellular localization.<sup>22</sup> As miR-29b contains a distinct hexanucleotide 3' motif that acts as a transferable NLS to direct nuclear enrichment, miR-29a/b/c variants were synthesized lacking the NLS (Figure 2a). NLS deletion from miR-29a/b/c enhanced their repression of *PSME4* (Figure 2d). Therefore, we reasoned that deletion of the miR-29b $\Delta$ NLS would increase cytoplasmic enrichment. 293T cells were transfected with lentivirus that expressed control miR, miR-29b or miR-29b $\Delta$ NLS, lysates prepared and nuclear and cytoplasmic fractions isolated. Northern blot analysis indicated that NLS deletion from miR-29b enriched cytoplasmic localization (Figure 2e).

MiR-29a, 29b and 29c replacements were transfected into myeloma cells and the effect on viability measured in RT (Figure 3a). The miR replacements reduced growth alone or combined with bortezomib. Deletion of the NLS from the miR-29a/b/c replacements further enhanced the inhibitory effect on growth in the presence of PIs (Figure 3b). To corroborate the antiproliferative effect of synthetically engineered miR-29 replacements, we employed expression vectors to generate miR-29a, -b or -c in myeloma cells. RPMI8226 cells were transduced with lentiviral vectors that expressed miR-29a, 29b or 29c and growth was measured in RT (Figure 3c). Similar to the synthetically engineered miR replacements, vector-based expression of miR-29b also reduced cell growth. We next investigated the miR-29b effect on the NF $\kappa$ B pathway, activated in tumor cells upon stress or chemotherapy to promote survival. As the level of miR-29b was reduced in PI-resistant cells, a synthetically

engineered miR-29b antagomir was employed to inhibit endogenous miR-29b. Transfection of the miR-29b antagomir increased NF $\kappa$ B activity, whereas miR-29b and miR-29b $\Delta$ NLS replacements reduced NF $\kappa$ B activity (Figure 3d). MiR-29b antagomirs also increased BrDU incorporation, whereas miR-29b replacements reduced incorporation (Figure 3e). MiR-29b replacement also reduced colony formation (Figure 3f) and increased the number of annexin-positive cells after PI treatment (Figure 3g). MiR-29b replacements also reduced the proliferation of other myeloma cell lines as well as cells from other malignant and nonmalignant B-cell types (Supplementary Figure 2).

PA200 functions in a variety of processes including proteasome assembly,<sup>23</sup> DNA repair,<sup>24</sup> genomic stability,<sup>25</sup> proteasome inhibition,<sup>26</sup> spermatogenesis<sup>27</sup> and mitochondrial checkpoint regulation<sup>28</sup> and stimulates the peptide-hydrolyzing activity of proteasomes. We reasoned that miR-29b reduction should reciprocally increase PA200 levels and enhance peptide-hydrolyzing activity of the proteasome. Lysates from PI-resistant cells were probed with western blot to indicate that PA200 levels were increased in PI-resistant cells compared with parental cells (Figure 4a). We hypothesized that synthetically engineered miR replacements could be exploited to inhibit *PSME4* and lead to reduced PA200 levels, proteasome inhibition and cell death. Parental and PI-resistant cells were transfected with control miR, miR-29b replacements or miR-29b $\Delta$ NLS replacements, cultured in the presence or absence of bortezomib and viability was determined (Figure 4b). PI-resistant cells transfected with miR-29b or miR-29b $\Delta$ NLS replacements were less viable than cells transfected with control miR. In addition, transfection of PI-resistant cells with miR-29b or miR-29b $\Delta$ NLS replacements enhanced their sensitivity to bortezomib. Hence, miR-29b replacement induced cytotoxicity either alone or in combination with bortezomib. We next determined the effect of miR-29b replacement on myeloma patient bone marrow-derived CD138<sup>+</sup> cells. The cells were transfected with control miR, miR-29b or miR-29b $\Delta$ NLS replacements, cultured for 24 h and treated with bortezomib. Bortezomib reduced the viability of patient CD138<sup>+</sup> cells and the effect was increased after transfection of miR-29b or miR-29b $\Delta$ NLS replacements (Figure 4c). RT-PCR demonstrated that miR-29b was reduced in PI-resistant cells and that miR-29b was reduced in patient CD138<sup>+</sup> cells relative to CD138<sup>+</sup> cells from healthy individuals (Figure 4d).

Whereas efficient substrate recognition by the proteasomal requires poly-Ub chain attachment to the targeted protein,<sup>29</sup> proteasomes also have the capacity to recognize and degrade substrates that do not require ubiquitination.<sup>30</sup> These include the cyclin-dependent kinase inhibitor p21, the transcriptional activator Rpn4 and ornithine decarboxylase (ODC).<sup>31</sup> To address the role of miR-29b on Ub-independent proteasome activity, PA200 null (PA200 $\Delta/\Delta$ ) lymphocytes were generated through Cre-loxP-mediated recombination.<sup>27</sup> PA200<sup>+/+</sup> and PA200 $\Delta/\Delta$  lymphocytes were then transfected with a vector that expressed GFP-ODC<sup>wt</sup>. PA200<sup>+/+</sup> and PA200 $\Delta/\Delta$  cells that expressed GFP-ODC<sup>wt</sup> were treated with cycloheximide and lysates were probed. Western blot analysis indicated that GFP-ODC<sup>wt</sup> was degraded much more rapidly in PA200<sup>+/+</sup> cells than in PA200 $\Delta/\Delta$  cells (Figure 5a). The half-life of GFP-ODC<sup>wt</sup> in PA200<sup>+/+</sup> cells was  $\sim 15$  min but was greater than 2 h in the PA200 $\Delta/\Delta$  cells.<sup>31</sup> PA200<sup>+/+</sup> and PA200 $\Delta/\Delta$  cells were transfected with miR-29b replacements to determine whether the miR-29b effect on proteasomes required PA200. Transfection of PA200 $\Delta/\Delta$  cells with control miR or miR-29b replacements did not change the GFP-ODC<sup>wt</sup> steady-state level (Figure 5b). However, transfection of miR-29b replacements into PA200<sup>+/+</sup> cells significantly increased the steady-state level of GFP-ODC<sup>wt</sup>, consistent with miR-29b replacement inhibiting *PSME4*, reducing PA200 and decreasing proteasome activity. The 20S proteasome core particle (CP) and the 26S proteasome (20S CP capped by 19S regulatory particles, RP-CP-RP) have been shown to

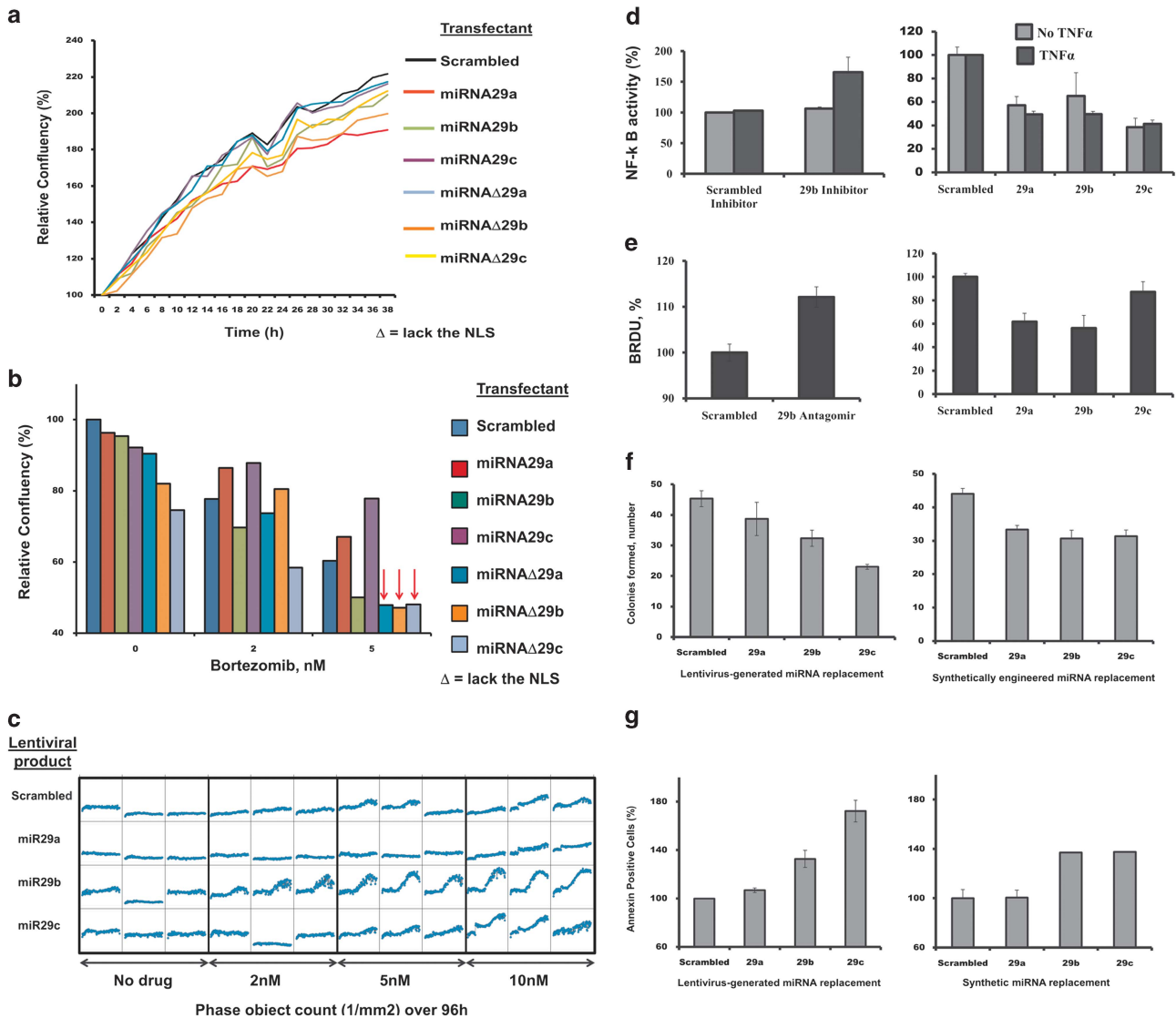


**Figure 3.** MiR-29b replacement effect on myeloma viability. **(a)** RT determination of miR-29 replacement on myeloma confluency. Cells were transfected with miRs (20 nM) and confluency determined in RT. **(b)** RT determination of miR-29 replacement effect on proliferation in the presence of bortezomib. Cells were transfected with indicated miRs (20 nM) and confluency determined in RT over 36 h at the indicated bortezomib concentrations. **(c)** Vector-based miR-29 replacement effect on myeloma cells in the presence of bortezomib. Cells were transfected with lentiviral vectors, selected with puromycin and the effect on viability was determined in the absence or presence of bortezomib at the indicated concentrations. **(d)** miR-29b effect on NF $\kappa$ B activity in the presence or absence of tumor necrosis factor- $\alpha$ . **(e)** miR-29b antagomir effect on proliferation. **(f)** miR-29 replacement effect on colony formation in methylcellulose (MC). MM cells were transfected with indicated miR replacements and the number of colonies counted after 7 days. Shown is the average of triplicate measurements. **(g)** MiR-29 replacement effect on the generation of annexin-positive cells in the presence of bortezomib. Myeloma cells were transfected with indicated miR replacements and the percentage of annexin-positive cells determined with flow cytometry. Cells transfected with control miR were normalized to 100% and the effect of each miR was determined.

associate with PA200 (refs 32,33). The 19S RP is responsible for selecting ubiquitinated proteins for degradation by the 20S CP. To investigate the impact of miR-29b replacement on proteasomes, myeloma cells were transfected with control miR or miR-29b replacements and either untreated or bortezomib treated. Lysates were fractionated, separated by nondenaturing gel electrophoresis and proteasome activity determined *in situ* upon incubation of the gel with the chymotrypsin-like substrate Suc-LLVY-MCA (Figure 5c). The *in situ* assay detected purified 26S (lane 1) and 20S proteasomes (lane 2). Control miR-transfected myeloma cells displayed two major peptide-hydrolyzing activities that migrated consistent with the 26S and 20S proteasome forms. However, these cells also contained at least three other peptide-

hydrolyzing activities that migrated between the 26S and 20S proteasomes (lane 3, indicated by \*). These activities may represent 20S CP hybrid proteasomes associated with a single RP and/or PA200. Proteasomes isolated from bortezomib-treated cells displayed reduced peptide-hydrolyzing activity independent of transfection with either control or miR-29b replacements (lanes 4, 6). Proteasomes from cells transfected with miR-29b replacements displayed reduced 26S proteasome peptide-hydrolyzing activity and lacked the three peptide-hydrolyzing activities that migrated between 26S and 20S proteasomes (lane 5). Thus, miR-29b replacement reduced the relative amount of peptide-hydrolyzing activity associated with 26S proteasomes. The proteasome hybrid forms that migrated below the 26S and

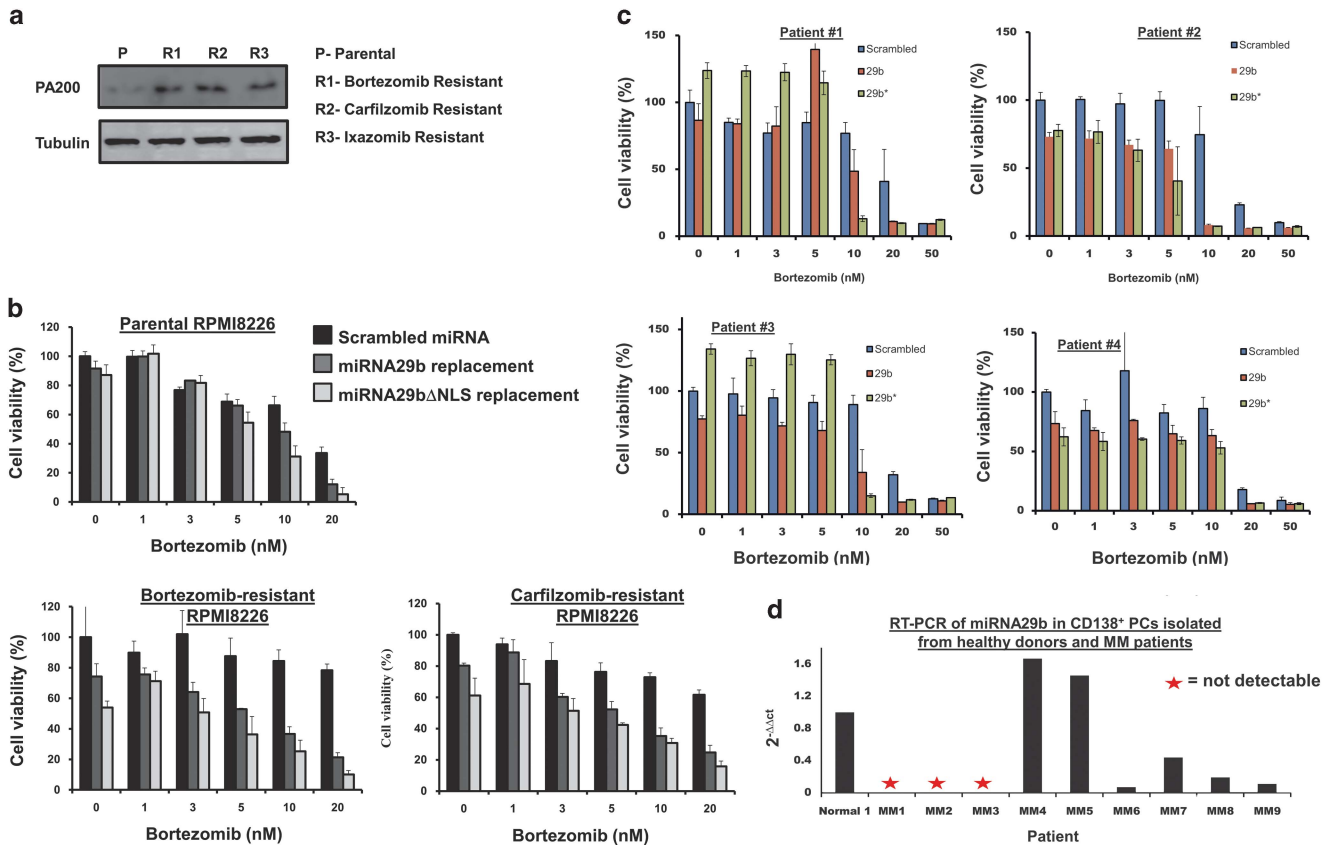


**Figure 4.** MiR-29b replacement effect on myeloma patient tumor samples. **(a)** Western blot of PA200 levels in parental and PI-resistant cells. Lysates from parental and PI-resistant cells were probed with an antibody specific to PA200. **(b)** Cytotoxic effect of control or miR-29b and miR-29b $\Delta$ NLS on parental and PI-resistant cells. Myeloma cells resistant to the PIs bortezomib or carfilzomib were transfected with the indicated miR replacements (20 nM) and the effect on viability determined using the XTT assay. **(c)** Effect of control or miR-29b on myeloma patient tumor cells. CD138<sup>+</sup> PCs from bone marrow (BM; ConversantBio, Huntsville, AL, USA) were isolated using microbead-positive selection (Miltenyi Biotec, Auburn, CA, USA). Samples were made > 85% pure by flow cytometry using an anti- $\alpha$ APC-labeled CD138<sup>+</sup> antibody. CD138<sup>+</sup> plasma cells were transfected with indicated miR replacements (20 nM) and the effect on cell viability determined using the XTT assay at 48 h. **(d)** RT-PCR of miR-29b in plasma cells isolated from BM of healthy individuals and MM patients. \* denotes that the product was not detectable by RT-PCR.

above the 20S proteasomes were also decreased after transfection of miR-29b replacements. The proteasome  $\beta$ 5 catalytic subunit (PSMB5) is a component of both 26S and 20S proteasomes. Therefore, western blot analysis with the PSMB5 antibody was used to determine the effect of miR-29b replacements on the relative amount of 26S and 20S proteasomes (Figure 5d). Lysates were prepared, fractionated, proteins separated by nondenaturing PAGE and probed by western blot. Proteasomes from control miR-transfected cells indicated PSMB5-immunoreactive bands that migrated similar to purified 26S and 20S proteasomes. Control miR-transfected cells also contained PSMB5-immunoreactive bands that migrated between the 26S and 20S proteasomes. However, proteasomes from cells transfected with miR-29 replacements demonstrated reduced PSMB5 staining at migration distances expected for the 26S proteasomes and proteasome that migrated between the 26S and 20S. Western blot analysis also indicated that PA200 association with 26S proteasomes was reduced in cells transfected with miR-29b replacements compared with control-transfected cells. Thus, miR-29b replacements reduced the relative amount of 26S proteasome activity and reduced the amount of PA200 associated with proteasomes.

As miR-29b replacements inhibited proteasome activity, we determined whether miR replacement, similar to bortezomib, induced the aggresome+autophagy pathway. Confocal microscopy

indicated that bortezomib treatment of control or miR-29b-transfected cells promoted Ub colocalization with the aggresome component histone deacetylase 6 (HDAC6), similar to the effect of bortezomib seen in prior studies.<sup>34,35</sup> p62/SQSTM1 is a Ub-binding protein and aggresome component that localizes with protein aggregates and bortezomib treatment increased p62 staining throughout the cytoplasm of both control and miR-29b-transfected cells. Protein aggregates within the cytoplasm are coalesced by microtubule-dependent retrograde transport to perinuclear deposition sites, referred to as aggresomes. Aggresomes are initially dispersed throughout the cytoplasm and subsequently travel on microtubules to the microtubule organizing center region, where they remain as distinct particulate structures entangled with collapsed intermediate filaments. We employed a novel, excitable red-fluorescent dye that specifically detects aggresomes. After bortezomib treatment, perinuclear aggresomes were readily detected in control-transfected cells but not in the miR-29b-transfected cells. The results suggest that miR-29b replacement enhances bortezomib-induced accumulation of protein aggregates but that these aggregates are not coalesced into perinuclear aggresomes. Bortezomib treatment also did not increase autophagosomes in the miR-29b-transfected cells as was seen in control-transfected cells.

Protein aggregation observed with miR-29b and bortezomib could result from inhibition of autophagy or lysosomal degradation

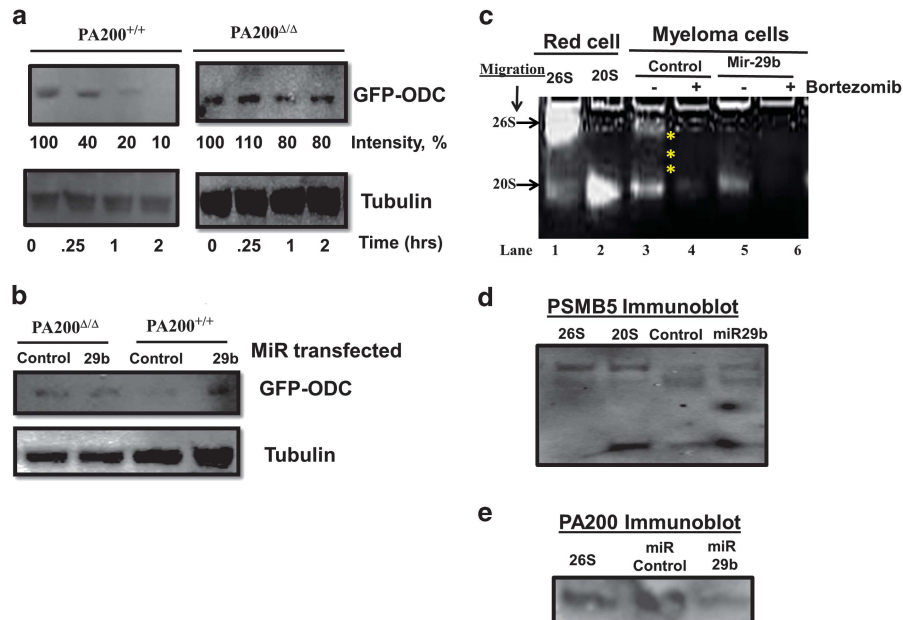


**Figure 5.** MiR-29b replacement affects PA200 association with proteasomes. **(a)** Effect of PA200 expression on GFP-ODC<sup>wt</sup> half-life. PA200<sup>+/+</sup> and PA200<sup>Δ/Δ</sup> cells were transfected with GFP-ODC<sup>wt</sup>, treated with cycloheximide and lysates were prepared at indicated time points. Lysates were separated with SDS-PAGE and probed using a GFP-specific antibody. **(b)** Effect of miR-29b on the steady-state level of GFP-ODC<sup>wt</sup> in PA200<sup>Δ/Δ</sup> and PA200<sup>+/+</sup> cells. Lymphocytes were transfected with control miR or miR-29b replacements, expanded and treated with bortezomib. Lysates were separated with SDS-PAGE and probed using a GFP-specific antibody. **(c)** MiR-29b replacement effect on proteasome activity. Purified human proteasomes (20S or 26S) or proteasomes isolated from myeloma cells were electrophoresed on Bio-Rad (Hercules, CA, USA) Criterion XT 4–20% Tris-Borate EDTA (TBE) gels run in TBE buffer (pH 8.3) at 4 °C and 25 V for 24 h. Nondenaturing 4% gel electrophoresis separated proteasomes isolated from the myeloma cells after transfection with either control miR or miR-29b. Chymotrypsin-like peptide hydrolyzing activity of proteasomes was determined by incubating the gel with Suc-LLVY-MCA. **(d)** MiR-29b replacement effect on proteasomes. Lysates from myeloma cells transfected with control miR or miR-29b replacements were separated by nondenaturing 4% PAGE, transferred to nitrocellulose and probed with western blot using an antibody to PSMB5 to determine the miR effect on the relative amount of the different proteasome forms. Purified 26S and 20S proteasomes (2 μg) were loaded separately as controls. Lysates from myeloma cells transfected with control miR or miR-29b replacements were separated by nondenaturing 4% PAGE, transferred to nitrocellulose and also probed using an antibody to PA200 to determine the miR effect on PA200 association with proteasomes.

of aggresomes late in the autophagy pathway. To distinguish between these possibilities, we investigated the effect of miR-29b replacements with or without bortezomib on LC3BII accumulation. Activation of autophagy results in LC3B lipidation that can be detected by faster migration on SDS-PAGE (as LC3BII). Western blot analysis indicated that both p62 and LC3BII increased when cells were treated with miR-29b and bortezomib (Figure 6b). However, because both p62 and LC3BII are degraded by autophagy, increased steady-state levels could result from either the activation or inhibition of autophagy. To discriminate between these possibilities, cells were treated with chloroquine during the last 30 min of incubation to suppress lysosomal-dependent protein degradation in autophagosomes. LC3BII accumulation occurred independent of bortezomib or miR-29b as well as in the presence or absence of chloroquine. As the increase in LC3BII occurred in untreated and treated cells, these data suggest that autophagy is active in these cells and unaffected by bortezomib, miR-29b or the combination. The results also suggested that miR-29b synergized with bortezomib to induce Ub-aggregate accumulation that was uncoupled from the formation of perinuclear aggresomes and autophagosomes. As miR-29b targeted PSME4, which encodes PA200, we determined the effect of PA200 knockout on aggresome formation (Figure 6c). Upon bortezomib treatment, we detected aggresomes and autophagosomes in PA200<sup>+/+</sup> cells but significantly reduced levels in PA200<sup>-/-</sup> cells (Figure 6c).

To determine the *in vivo* effect of miR-29b replacement, lentiviral vectors that expressed control, miR-29b or miR-29bΔNLS were transfected into RPMI8226 cells that were then injected into

the flanks of NOD.CB17-Prkdcscid/J mice (Figure 7a). Mice injected with control miR-transduced cells developed tumors earlier than the other groups, and tumor volumes increased more than those generated using cells transduced with miR-29b or miR-29bΔNLS. Survival of mice injected with cells transduced with miR-29b or miR-29bΔNLS was also significantly longer compared with mice injected with control cells (Figure 7b). Imaging indicated that the flanks of mice injected with cells expressing control miR emitted greater fluorescence than flanks of mice injected with cells expressing miR-29b or miR-29bΔNLS (Figure 7c).

## DISCUSSION

The UPS is an attractive therapeutic target because of its stringent regulation of pro-survival and anti-apoptotic regulators. Bortezomib represents a remarkable bench-to bedside success but sustained response is hindered by drug resistance. We identified miRs deregulated in PI-resistant cells and establish a compelling link between miRs and PI resistance.<sup>34–36</sup> A diversity of mechanisms has been proposed to explain how malignant cells escape PIs, including alterations in the proteasome itself.<sup>37,38</sup> For example, in myelomonocytic cell lines, mutations in the proteasome catalytic subunit PSMB5 impair bortezomib binding and PSMB5 is upregulated following bortezomib exposure. PSMB5 induction wanes with time off-therapy, but reappears rapidly after drug re-exposure to highlight the susceptibility of proteasomes to genetic modifications under selection pressure, as may occur in patients with continued treatment. Our results provide a proof-of-principle to demonstrate that miRs offer potential as novel therapeutic



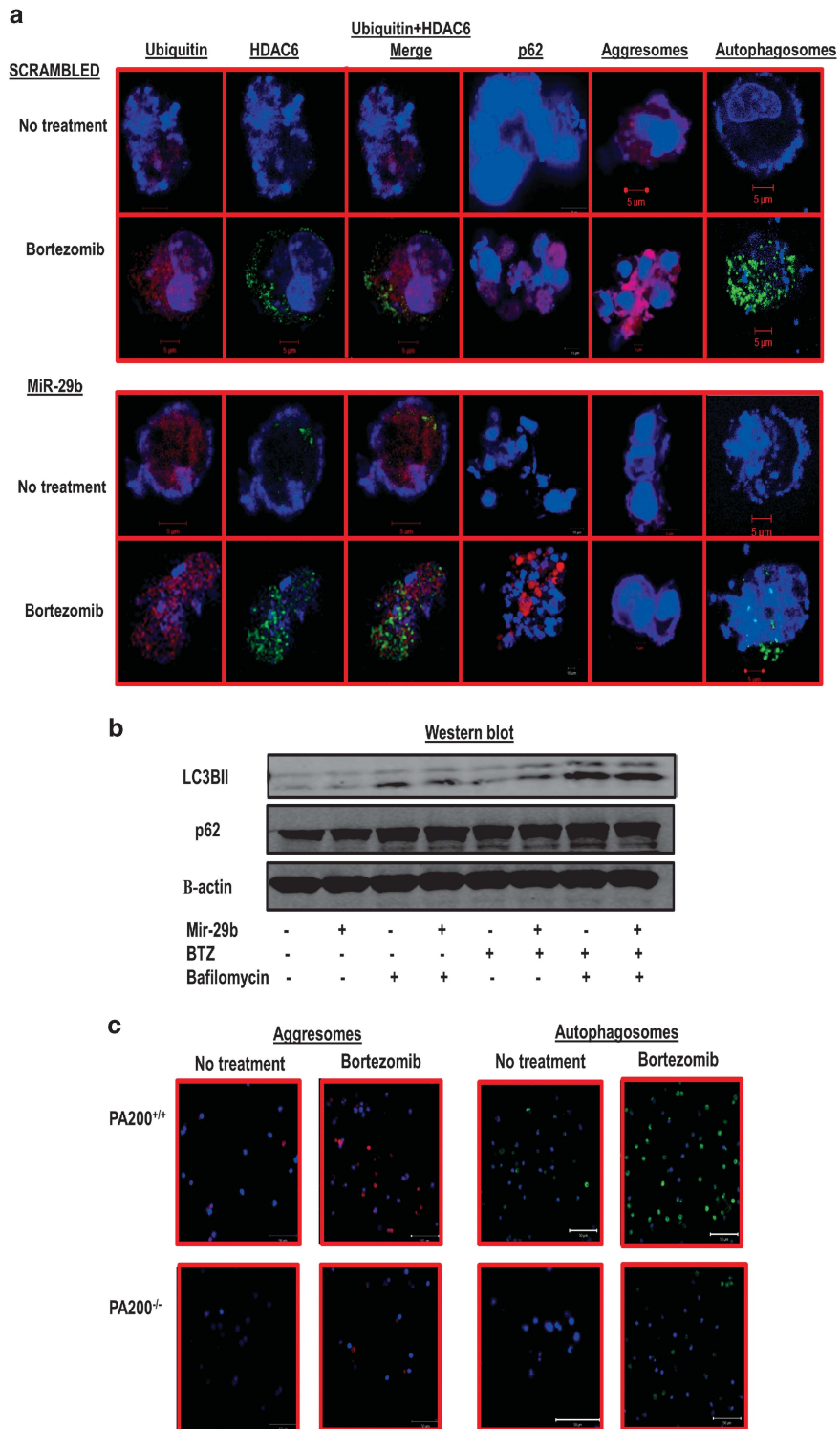


**Figure 6.** MiR-29b replacement affects on aggresome and autophagy formation. (a) Immunofluorescent colocalization of Ub, p62 and HDA6 in RPMI8226 cells. Cells were transfected with control miR or miR-29b replacements and treated with bortezomib for 16 h. Images were visualized using a Zeiss LSM 170 confocal microscope (Zeiss Microscopy) with Axio Observer Z1. Aggresomes were visualized using the Enzo Proteostat aggresome detection kit (Enzo Life Sciences, Farmingdale, NY, USA). Autophagosomes were detected using the Cyto-ID autophagy detection kit (Enzo Life Sciences) according to the manufacturer's instructions. (b) Western blot of p62 and LC3B in RPMI8226 cells transfected with either control miR or miR-29b and treated with bortezomib. Cells were treated with chloroquine for the final 30 min of incubation to allow for autophagosome accumulation. (c) Aggresome and autophagosome formation in PA200<sup>+/+</sup> and PA200<sup>-/-</sup> cells. Cells were treated with bortezomib and aggresomes and autophagosomes detected using the Enzo detection kits.

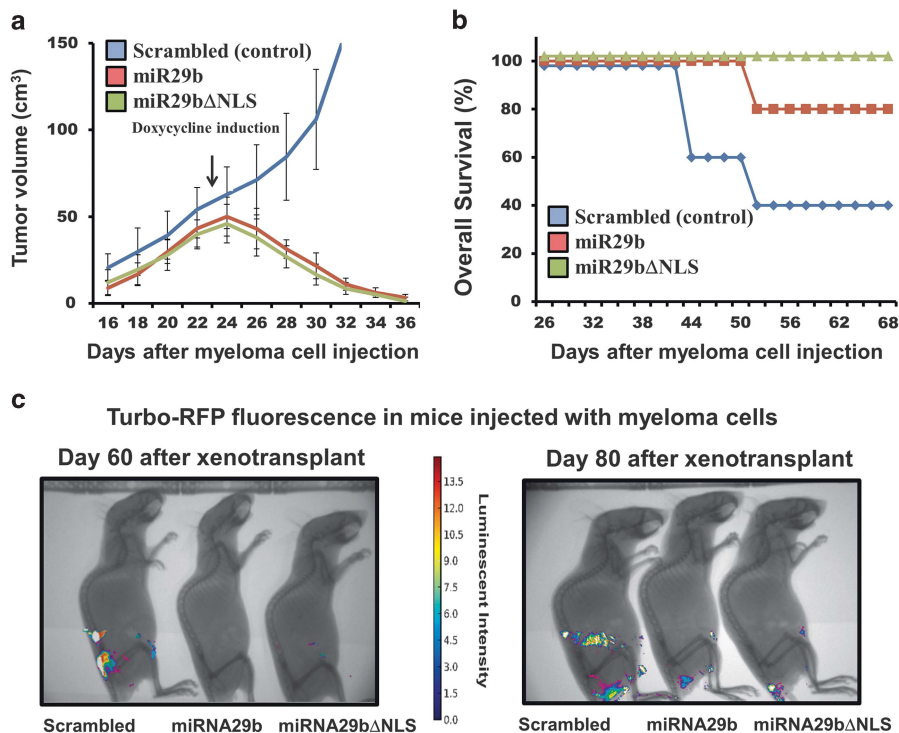


**Figure 7.** *In vivo* effect of miR-29b replacements on myeloma xenotransplants. (a) Effect of miR-29b and miR-29bΔNLS on tumor volume of myeloma xenotransplants. The TRIPZ inducible lentiviral system was used to express control or miR-29b in MM cells before their subcutaneous xenotransplantation into NOD/SCID female mice. The TRIPZ-inducible system employed a doxycycline-inducible promoter. The TRE, modified from its natural state to consist of a string of operators fused to the CMV minimal promoter, reduced the basal expression and tighter binding to the second component, the transactivator. The pTRIPZ transactivator, known as the reverse tetracycline transactivator, binds and activates expression from TRE promoters in the presence of doxycycline. Mutations within the rtTA increase sensitivity to doxycycline by 25-fold over the initial rtTA without increasing background.<sup>51</sup> Cells ( $3 \times 10^6$ ) transduced with lentivirus expressing either control, miR-29b or miR-29bΔNLS were subcutaneously injected into the flanks of 5-week-old, female NOD.CB17-Prkdcscid/J mice, with five mice/group. After detection of measurable ( $> 50 \text{ mm}^3$ ) tumors, mice were started on an alfalfa-free diet supplemented with doxycycline (Dox) to enhance pTRIZ promoter expression. Tumor volume was determined by external measurement using electronic calipers. Each group contained five mice and the mice were injected in each flank. Shown is the average of replicate measurements from the five mice in each group. Subcutaneous tumor volume was determined by obtaining external measurements with a digital caliper using the modified ellipsoidal formula: tumor volume =  $\frac{1}{2}$  (length  $\times$  width<sup>2</sup>). (b) Effect of miR-29b and miR-29bΔNLS on overall survival. The *in vivo* efficacy of lentiviral-delivered miR-29b replacements on the viability of NOD/SCID mice was determined over 10 weeks after subcutaneous injection. Overall survival of the mice that were injected with MM cells transfected with either the scrambled or the experimental miRs. (c) Effect of miR-29b and miR-29bΔNLS on tumor size by fluorescence imaging of TurboRFP-expressing cells implanted subcutaneously on the flanks of NOD.CB17-Prkdcscid/J mice. Shown is a representative mouse from each group of five mice. Imaging was completed using the *in vivo* MultiSpectral FX Pro (Bruker Biospin, Billerica, MA, USA) in the Vontz Core Imaging Laboratory. TurboRFP fluorescence was captured with the IS400MM camera with 550 nm excitation filter and 600 nm emission filter. Images were acquired for 10 s with  $4 \times 4$  binning and data were processed with the Carestream software (Rochester, NY, USA).

agents to inhibit proteasomes and provide an alternative strategy to disrupt the UPS (Figure 8). Profiling of patient tumor cells to quantitate miR levels may provide useful information to predict the response to bortezomib. In addition, we envision the development of a panel of miRs that correlate with drug response as a signature for use in clinical practice to identify those patients less likely to respond to bortezomib-based therapy. These patients could then be treated upfront with more aggressive therapies.

Whereas it is reasonable to assume that miR-29b targets multiple mRNAs, a number of observations are consistent with a direct effect on *PSME4*. MiR-29b antagonists increased proteasomal degradation of GFPu and miR-29b replacements inhibited *PSME4* expression, reduced PA200 levels and decreased PA200 association with proteasomes. Proteasomes isolated from cells transfected with miR-29b replacements displayed reduced peptidase activity. PA200-CP complexes were observed under stress conditions to also suggest that PA200 increases proteasome activity.<sup>33,39</sup> Substrates access the central chamber of the proteasome through narrow gates defined by the outer  $\alpha$ -rings of the 20S CP. In the absence of activators, these gates are closed

by the 20S- $\alpha$  subunits that forge these rings to repress proteolysis rates.<sup>33</sup> Three-dimensional molecular structures determined with X-ray crystallography of CP-bound Blm10 (the yeast PA200 homolog) have provided a model for gate-opening and activation.<sup>33</sup> PA200/Blm10 inserts into a dedicated pocket in the outer ring of the CP surface to induce and stabilize a partially open gate conformation. MiR-29b reduction also enhanced Ub-independent degradation to support the concept that short-lived proto-oncogenes, onco-suppressive proteins and core histones are degraded through Ub-independent, proteasome-dependent mechanisms.<sup>40</sup> PA200 may direct the degradation of specific protein classes or direct localized proteasome degradation.

We demonstrate that miR-29b replacements combined with bortezomib enhance the accumulation of protein aggregates but that aggresome and autophagosome formations were impaired and that uncoupling toxic protein accumulation from the aggresome+autophagy pathways enhances the cytotoxic effect of bortezomib. HDAC inhibitors combined with bortezomib also inhibit aggresome formation and increase the apoptotic effect of

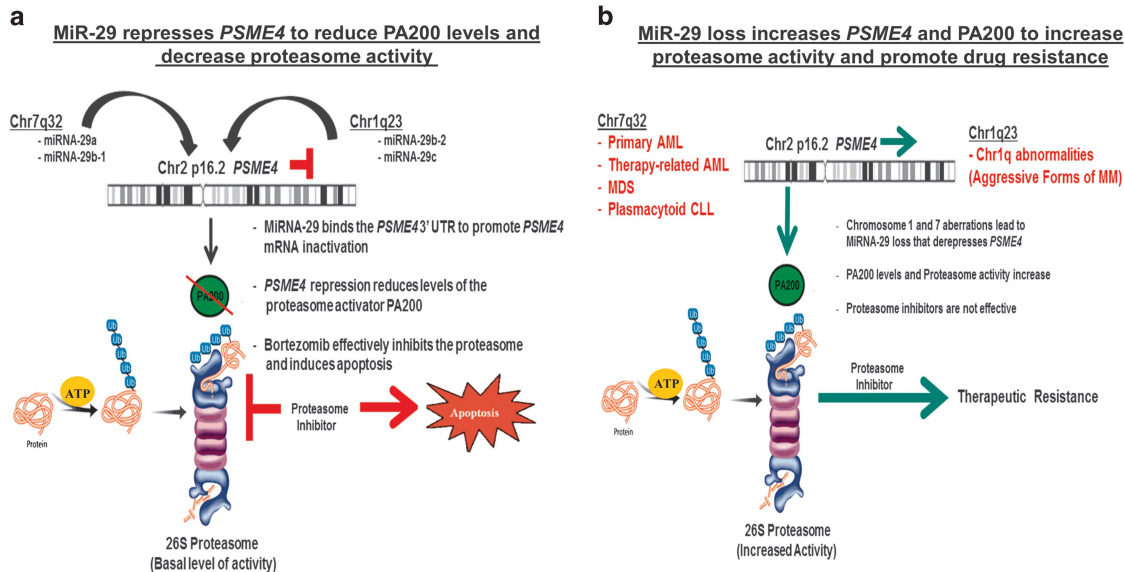


**Figure 8.** Model depicting the effect of miR-29 on *PSME4*, PA200, proteasomes and cellular sensitivity to bortezomib. (a) miR-29a and 29b1 (from chromosome 1) and miR29b-2 and 29c (from chromosome 7) bind the *PSME4* 3'-UTR leading to a reduction in proteasome activator PA200 levels. Cells exhibit a basal level of proteasome activity that is readily inhibited by PIs and leads to apoptosis. (b) Loss of miR-29 family members through chromosomal translocation or other genetic abnormalities increases *PSME4* expression and PA200 levels to increase proteasome activity and render cells therapeutically resistant to PIs.

the drug.<sup>41–43</sup> Likewise, the farnesyl transferase inhibitor lonafarnib (tipifarnib) synergizes with bortezomib to enhance the accumulation of ubiquitinated proteins. The efficient packaging of proteins into aggresomes is clearly important in the cells' ability to manage misfolded proteins but must be coupled with efficient delivery of the aggresome to autophagosomes.<sup>44</sup> The therapeutic use of miRs has gained much attention because their mechanisms of action are consistent with the current approach to treat cancer as a pathway-based disease. MiRs are master regulators of the genome that modulate hundreds of genes and control multiple essential cellular pathways. Thus, miR-based therapeutics are highly applicable to a molecularly heterogeneous disease with distinct genetic subtypes, for example, MM and B-cell disorders.<sup>45–47</sup> A number of miRs, including miR-29b, show a loss of function in a broad range of cancer types, indicating that they have a central role in regulating tumor suppression.<sup>48,49</sup> Correcting these deficiencies by miR replacement results in the activation of pro-apoptotic pathways. Since the groundbreaking discovery that miRs were aberrantly expressed in cancers, significant progress has advanced the clinical development as diagnostics and therapeutics.<sup>50</sup>

## CONFLICT OF INTEREST

The authors declare no conflict of interest.

## ACKNOWLEDGEMENTS

We thank Driscoll laboratory members for critical reading of the manuscript.

## REFERENCES

- Ameres SL, Zamore PD. Diversifying microRNA sequence and function. *Nat Rev Mol Cell Biol* 2013; **14**: 475–488.
- Tay Y, Rinn J, Pandolfi PP. The multilayered complexity of ceRNA crosstalk and competition. *Nature* 2014; **505**: 344–352.
- Calin GA, Croce CM. MicroRNA signatures in human cancers. *Nat Rev Cancer* 2006; **6**: 857–866.
- Esquela-Kerscher A, Slack FJ. Oncomirs—microRNAs with a role in cancer. *Nat Rev Cancer* 2006; **6**: 259–269.

- Song SJ, Ito K, Ala A, Kats L, Webster K, Sun SM *et al*. The oncogenic microRNA miR-22 targets the TET2 tumor suppressor to promote hematopoietic stem cell self-renewal and transformation. *Cell Stem Cell* 2013; **13**: 87–101.
- Bader AG, Brown D, Winkler M. The promise of microRNA replacement therapy. *Cancer Res* 2010; **70**: 7027–7030.
- Gallastegui N, Groll M. The 26S proteasome: assembly and function of a destructive machine. *Trends Biochem Sci* 2010; **35**: 634–642.
- Richardson PG, Sonneveld P, Schuster MW, Irwin D, Stadtmauer EA, Facon T *et al*. Assessment of Proteasome Inhibition for Extending Remissions (APEX) investigators. Bortezomib or high-dose dexamethasone for relapsed multiple myeloma. *N Engl J Med* 2005; **352**: 2487–2498.
- Hideshima T, Richardson P, Chauhan D, Palombella VJ, Elliott PJ, Adams J *et al*. The proteasome inhibitor PS-341 inhibits growth, induces apoptosis, and overcomes drug resistance in human multiple myeloma cells. *Cancer Res* 2001; **61**: 3071–3076.
- Palumbo A, Anderson K. Multiple myeloma. *N Engl J Med* 2011; **364**: 1046–1060.
- Nalepa G, Rolfe M, Harper W. Drug discovery in the ubiquitin-proteasome system. *Nat Rev Drug Discov* 2006; **5**: 596–613.
- Richardson PG, Schlossman RL, Alsina M, Weber DM, Coutre SE, Gasparetto C *et al*. PANORAMA 2: panobinostat in combination with bortezomib and dexamethasone in patients with relapsed and bortezomib-refractory myeloma. *Blood* 2013; **122**: 2331–2337.
- Orlowski R. Why proteasome inhibitors cannot ERADicate multiple myeloma. *Cancer Cell* 2013; **24**: 275–277.
- Leung-Hagesteijn C, Erdmann N, Cheung G, Keats JJ, Stewart AK, Reece DE *et al*. Xbp1s-negative tumor B cells and pre-plasmablasts mediate therapeutic proteasome inhibitor resistance in multiple myeloma. *Cancer Cell* 2013; **24**: 289–304.
- Bence NF, Bennett EJ, Kopito RR. Application and analysis of the GFPu family of ubiquitin-proteasome system reporters. *Methods Enzymol* 2005; **399**: 481–490.
- Badr CE, Niers JM, Tjon-Kon-Fat LA, Noske DP, Wurdinger T, Tannous BA *et al*. Real-time monitoring of nuclear factor kappaB activity in cultured cells and in animal models. *Mol Imaging* 2009; **8**: 278–290.
- Tannous BA. Gaussia luciferase reporter assay for monitoring of biological processes in culture and *in vivo*. *Nat Protoc* 2009; **4**: 582–591.
- Volinia S, Calin GA, Liu CG, Ambs S, Cimmino A, Petrocca F *et al*. A microRNA expression signature of human solid tumors defines cancer gene targets. *Proc Natl Acad Sci USA* 2006; **103**: 2257–2261.
- Migliore C, Giordanom S. Resistance to targeted therapies: a role for microRNAs? *Trends Molecular Medicine* 2013; **19**: 633–642.
- Bence NF, Sampat RM, Kopito RR. Impairment of the ubiquitin-proteasome system by protein aggregation. *Science* 2011; **292**: 1552–1555.

- 21 Liu S, Wu L-C, Pang J, Santhanam R, Schwind S, Wu Y-Z. Sp1/NFκB/HDAC/miR-29b regulatory network in KIT-driven myeloid leukemia. *Cancer Cell* 2010; **17**: 333–347.
- 22 Hwang HW, Wentzel EA, Mendell JT. A hexanucleotide element directs microRNA nuclear import. *Science* 2007; **315**: 97–100.
- 23 Fehhler M, Wendlner P, Lehmann A, Enekel C. Bim3 is part of nascent proteasomes and is involved in a late stage of nuclear proteasome assembly. *EMBO Rep* 2003; **4**: 959–963.
- 24 Schmidt M, Haas W, Crosas B, Santamaria PG, Gygi SP, Walz T *et al*. The HEAT repeat protein Bim10 regulates the yeast proteasome by capping the core particle. *Nat Struct Mol Biol* 2005; **12**: 294–303.
- 25 Blickwedehl J, Agarwal M, Seong C, Pandita RK, Melendy T, Sung P *et al*. Role for proteasome activator PA200 and postglutamyl proteasome activity in genomic stability. *Proc Natl Acad Sci USA* 2008; **105**: 16165–16170.
- 26 Lehmann A, Jechow K, Enekel C. Bim10 binds to pre-activated proteasome core particles with open gate conformation. *EMBO Rep* 2008; **9**: 1237–1243.
- 27 Khor B, Bredemeyer AL, Huang CY, Turnbull IR, Evans R, Maggi LB *et al*. Proteasome activator PA200 is required for normal spermatogenesis. *Mol Cell Biol* 2006; **26**: 2999–3007.
- 28 Sadre-Bazzaz K, Whitby FG, Robinson H, Formosa T, Hill CP. Structure of a Bim10 complex reveals common mechanisms for proteasome binding and gate opening. *Mol Cell* 2010; **27**: 728–735.
- 29 Thrower JS, Hoffman L, Rechsteiner M, Pickart CM. Recognition of the poly-ubiquitin proteolytic signal. *EMBO J* 2000; **19**: 94–102.
- 30 Verma R, Deshaies RJ. A proteasome howdunit: The case of the missing signal. *Cell* 2000; **101**: 341–344.
- 31 Ghoda L, van Daalen Wetters T, Macrae M, Ascherman D, Coffino P. Prevention of rapid intracellular degradation of ODC by a carboxyl-terminal truncation. *Science* 1989; **243**: 1493–1495.
- 32 Stadtmueller BM, Hill CJ. Proteasome activators. *Mol Cell* 2011; **41**: 8–19.
- 33 Savulescu AF, Glickmann M. Proteasome activator 200: the heat is on. *Mol Cell Proteomics* 2011; **10**: R110.006890.
- 34 Chauhan D, Tian Z, Zhou B, Kuhn D, Orlowski R, Raje N *et al*. *In vitro* and *in vivo* selective antitumor activity of a novel orally bioavailable proteasome inhibitor MLN9708 against multiple myeloma cells. *Clin Cancer Res* 2011; **17**: 5311–5321.
- 35 Siegel DS, Martin T, Wang M, Vij R, Jakubowiak AJ, Lonial S *et al*. A phase 2 study of single-agent carfilzomib (PX-171-003-A1) in patients with relapsed and refractory multiple myeloma. *Blood* 2012; **120**: 2817–2825.
- 36 Dick LR, Fleming PE. Building on bortezomib: second-generation proteasome inhibitors as anti-cancer therapy. *Drug Discov Today* 2010; **15**: 243–249.
- 37 Kumar S, Rajkumar SV. Many facets of bortezomib resistance susceptibility. *Blood* 2008; **112**: 2177–2178.
- 38 Oerlemans R, Franke NE, Assaraf YG, Cloos J, van Zantwijk I, Berkens CR *et al*. Molecular basis of bortezomib resistance: proteasome subunit beta5 (PSMB5) gene mutation and overexpression of PSMB5 protein. *Blood* 2008; **112**: 2489–2499.
- 39 Book AJ, Gladman NP, Lee SS, Scaff M, Smith LM, Vierstra RD. Affinity purification of the Arabidopsis 26S proteasome reveals a diverse array of plant proteolytic complexes. *J Biol Chem* 2010; **285**: 25554–25569.
- 40 Hoyt MA, Coffino P. Ubiquitin-free routes into the proteasome. *Cell Mol Life Sci* 2004; **61**: 1596–1600.
- 41 Hideshima T, Bradner JE, Wong J. Small molecule inhibition of proteasome and aggresome function induces synergistic antitumor activity in multiple myeloma. *Proc Natl Acad Sci USA* 2005; **102**: 8567–8572.
- 42 Catley L, Weisberg E, Kiziltepe T, Tai YT, Hideshima T, Neri P *et al*. Aggresome Induction by proteasome inhibitor bortezomib and α-tubulin hyperacetylation by tubulin deacetylase (TDAC) inhibitor LBH589 are synergistic in myeloma cells. *Blood* 2006; **108**: 3441–3449.
- 43 Harrison SJ, Quach H, Link E, Seymour JF, Ritchie DS, Ruell S *et al*. A high rate of durable responses with romidepsin, bortezomib, and dexamethasone in relapsed or refractory multiple myeloma. *Blood* 2011; **118**: 6274–628340.
- 44 David E, Kaufman JL, Flowers CR, Schafer-Hales K, Torre C, Chen J, Marcus AI, Sun SY, Boise LH, Lonial S. Tipifarnib sensitizes cells to proteasome inhibition by blocking degradation of bortezomib-induced aggresomes. *Blood* 2010; **116**: 5285–5288.
- 45 Roccaro AM, Sacco A, Chen C, Runnels J, Leleu X, Azab F *et al*. microRNA expression in the biology, prognosis, and therapy of Waldenstrom macroglobulinemia. *Blood* 2009; **113**: 4391–4402.
- 46 Roccaro AM, Sacco A, Thompson B, Leleu X, Azab AK, Azab F *et al*. MicroRNAs 15a and 16 regulate tumor proliferation in multiple myeloma. *Blood* 2009; **13**: 6669–6680.
- 47 Morgan GJ, Walker BA, Davies FE. The genetic architecture of multiple myeloma. *Nat Rev Cancer* 2012; **12**: 335–348.
- 48 Bader AG. miR-34- a microRNA replacement therapy is headed to the clinic. *Front Genet* 2012; **3**: 1–9.
- 49 Wiggins JF, Ruffino L, Kelnar K, Omotola M, Patrawala L, Brown D *et al*. Development of a lung cancer therapeutic based on the tumor suppressor microRNA-34. *Cancer Res* 2010; **70**: 5923–5930.
- 50 Ahmad N, Haider S, Anaissie E, Driscoll JJ. MicroRNA theragnostics for the clinical management of multiple myeloma. *Leukemia* 2014; **28**: 732–738.
- 51 Das AT, Zhou X, Vink M, Klaver B, Verhoef K, Marzio G *et al*. Viral evolution as a tool to improve the tetracycline-regulated gene expression system. *J Biol Chem* 2004; **229**: 18776–18782.



This work is licensed under a Creative Commons Attribution-NonCommercial-ShareAlike 4.0 International License. The images or other third party material in this article are included in the article's Creative Commons license, unless indicated otherwise in the credit line; if the material is not included under the Creative Commons license, users will need to obtain permission from the license holder to reproduce the material. To view a copy of this license, visit <http://creativecommons.org/licenses/by-nc-sa/4.0/>

Supplementary Information accompanies this paper on the Leukemia website (<http://www.nature.com/leu>)